Laboratory studies of ship hull's material degradation scenarios to optimize a cathodic protection modelling software

Marie Minola, Virginie Roche, Laure-Line Rouve, Olivier Pinaud, Olivier Chadebec, Michaël Nale, Cédric Goëau, Jean-Claude Lepretre

ARTICLE OPEN

Check for updates

Laboratory studies of ship hull's material degradation scenarios to optimize a cathodic protection modelling software

Marie Minola[1]✉, Virginie Roche[1]✉, Laure-Line Rouve[2], Olivier Pinaud[2], Olivier Chadebec[2], Michaël Nale[2], Cédric Goëau[3] and Jean-Claude Lepretre[1]

This work presents the experimental research carried out to optimize a current computational software "CorOns", to obtain a better ship hull electrical signature modelling. Middle-term ageing (597 days) of anticorrosion paints, highlights the appearance of additional corrosion processes, despite an absence of visual defects. A specific model is proposed for an aged surface in seawater based on Electrochemical Impedance Spectroscopy ("EIS") data analysis. We also investigate the impact of the interruption of cathodic protection on the corrosion process, with the objective of modelling the electrical signature in real conditions that could be encountered. These studies' interruption of the cathodic protection during 24 h, do not seem to have an impact on the current densities. However, EIS studies, highlight that the protection interruptions damage the calcareous deposit, well-known for it is protective effect once formed.

npj Materials Degradation (2023)7:24 ; https://doi.org/10.1038/s41529-023-00341-w

INTRODUCTION

In recent decades, research for the optimization of corrosion protection systems has focused on both the reduction of energy consumption and the electromagnetic discretion of ships[1–4]. The main sources of the electromagnetic signature of ships is corrosion processes and corrosion protection systems[1–3].

Because of these processes, naval vessels can be detected especially with new generation of weapons such as the so-called "smart-mine", developed since World War II. Therefore, over the last decades, many research projects have been working to reduce this signature with cathodic protection system optimization thanks to computational tools[3–6].

To protect ships from natural corrosion processes, several layers of anticorrosion paint are used as well as the Impressed Current Cathodic Protection (ICCP) and Galvanic Anode (GACP) in the most sensitive areas. Two conditions are identified as sources of electric fields in the hull environment of ships:

- Natural process of galvanic corrosion between less noble areas of the hull (defects) considered as anodic part and the propellers or bow thrusters, which are usually made of more noble materials forming the cathode electrodes (Fig. 1A). For example, Nickel Aluminum Bronze (NAB), are often used as propeller material.
- Under cathodic protection conditions when an electric field is emitted from the injection anodes and/or galvanic anodes to metallic areas (propellers or defects on the hull represented by unpainted steel) (Fig. 1B).

Numerical modelling of the propagation of electromagnetic fields[1–3,5–9] often gives a representative prediction of the electromagnetic signature of ships. The CorOns solver, based on the Boundary Element Method has been developed in this context by the G2elab laboratory. The novelty of this solver is the coupling of BEM method with equivalent circuit[7,8]. Like many modelling software, it demands experimental studies especially for the interfaces' representation and their evolution according to different corrosion scenarios encountered in real conditions.

Among the different scenarios investigated, the behavior of hull under natural and accelerated ageing conditions is studied with a focus on the unpainted area (defects). These results will be integrated as boundary conditions in the computational software "CorOns"[7,8]. One of the points discussed in this article, is the verification of certain assumptions generally used in modelling software to represent the different metal/electrolyte interfaces under cathodic protection. The verifying assumption presented here, concerns the painted steel modelling by a pure insulator when no visible defect is observed (i.e., unpainted area)[2,3,10].

The novelty of this presented article concerns the evolution of the well-known calcareous deposit under cathodic protection interruptions. The behavior of steels, often carbon steel for hull application, in marine environment under cathodic protection, has already been the subject of numerous studies[11–17]. However, rarely studies are focused on the impact of the cathodic protection interruption on the electrochemical behavior of the interface. The idea is to evaluate if this calcareous deposit, whose protective properties by "barrier effect", could be improved according to the "pulse method effect" described by Zamanzade et al.[18]. This can represent another source of electrical signature modification of the vessels.

In this context, electrochemical impedance spectroscopy (EIS) under cathodic polarization and potentiodynamic polarization curves and potentiostatic measurements are carried out associated with spectroscopic investigation allowing to characterizing the undamaged and damaged hull in synthetic seawater.

RESULTS AND DISCUSSION

In this part, the exploitation of impedance diagrams with the development of Electrical Equivalent Circuits "EEC" model, are

[1]Univ. Grenoble Alpes, Univ. Savoie Mont Blanc, CNRS, Grenoble INP (Institute of Engineering and Management Univ. Grenoble Alpes), LEPMI, 38402 Saint Martin d'Hères, France. [2]Univ. Grenoble Alpes, CNRS, Grenoble INP (Institute of Engineering and Management Univ. Grenoble Alpes), G2Elab, 38000 Grenoble, France. [3]DGA/GESMA, Département DDBF BP 42, 29240 Brest Armées, France. ✉email: marie.minola@grenoble-inp.fr; virginie.roche@grenoble-inp.fr

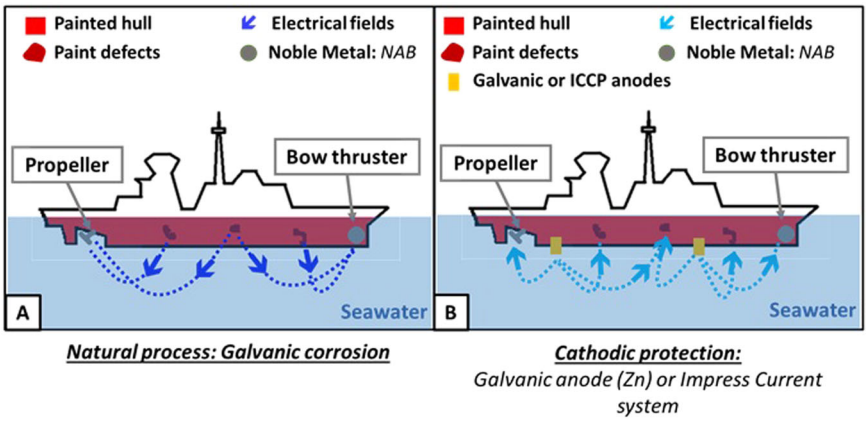

Fig. 1 Illustration of the major causes of electrical signature of ship's hull. There are two cases, the natural and spontaneous phenomenon, the galvanic coupling illustrated in (**A**), and the process of cathodic protection illustrated in (**B**) with the case of Impress Current Cathodic Protection system (ICCP)[4].

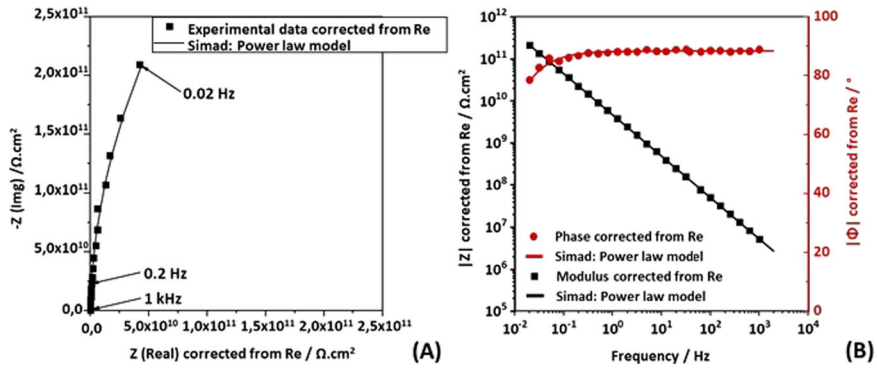

Fig. 2 Nyquist diagram and Bode diagram of undamaged painted steel. The imaginary part (Z(img)) is plotted in function of the real part (Z(Re)) of the impedance for the Nyquist diagram in (**A**). The modulus (black curve) and phase (red curve) are plotted in function of the frequency in (**B**). Both diagrams are corrected by the Re (Electrolyte resistance), with the modelling result obtained from the EEC presented in (Fig. 3, straight lines) and the power low model implemented in the SIMAD® software, at 20 °C under static condition and in naturally aerated solution.

presented, in order to distinguish the various phenomena at metal/electrolyte interfaces and their evolution.

Freshly painted DH36 steel without defect

The Nyquist Diagram in Fig. 2A, illustrates a high capacitive behavior with imaginary part of the impedance higher than 200 GΩ.cm^2 at 20 mHz in agreement with several works[19,20], suggesting high protective properties of the coating. Furthermore, the semicircle shape of the Nyquist diagram confirms the presence of a resisto-capacitive phenomenon presented on the proposed equivalent model Fig. 3. This observation is confirmed with the Bode diagram in Fig. 2B, which is corrected from the ohmic drop considered as equal to electrolyte resistance "Re"[21].

A constant phase close to 90° between 50 Hz and 10 kHz (Fig. 2) is observed, which suggested a capacitive behavior[19,20]. This assumption is supported by the very high modulus values obtained in the same frequency domain: from 10 MΩ.cm^2 (10 kHz) to 10 GΩ.cm^2 (50 Hz) and higher below 50 Hz. The high modulus of over 10 GΩ.cm^2 at high frequency (10 kHz) suggests that the paint layer and its strongly protective dielectric properties can mask other electrochemical processes despite the ohmic drop corrections in the diagram. That is why, in our equivalent model (Fig. 3, Electrical Equivalent Circuit model, EES), only one time constant related to the dielectric properties of the paint is considered as faradic phenomena is not observed (double-layer capacitance and transfert resistance). These observations are in good agreement with a freshly painted anticorrosion protective coating behavior has reported in other studies[19,20,22]. In this case, it is possible to modelling this interface by a single resisto-capacitive phenomenon (Fig. 3).

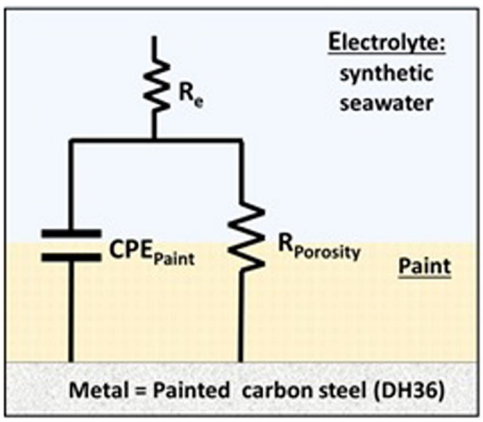

Fig. 3 Equivalent Electrical Circuit (EEC) of a freshly painted steel/seawater interface. It illustrates the case of a freshly painted, defect-free sample immersed in seawater after 2 h at OCP (Open Circuit Potential), at 20 °C in static condition and natural aeration.

Furthermore, the single slope close to unity for the modulus vs frequency (Fig. 2B) and the independence of the phase with the frequency is typical of a CPE (Constant Phase Element) behavior[21].

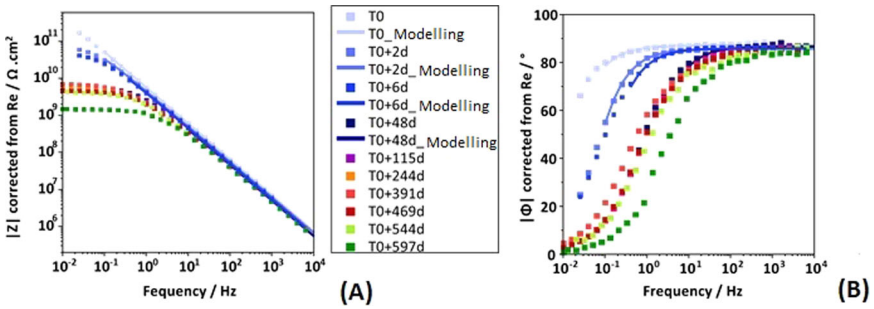

Fig. 4 Bode diagrams obtained regularly during 597 days of painted DH36 steel immersed in seawater. The modulus in (**A**) and phase in (**B**) are plotted as a function of frequency, in artificial seawater at 20 °C, under natural aeration and static conditions.

CPE is often used to accommodate heterogeneities at the interface and especially in our case; it can refer to thickness heterogeneities of the paint leading to a time constant dispersion. In this case, a normal dispersion has been considered with the use of the Power-Law model[23] to model this CPE (Eq. 1).

$$Z_i(\omega) = \int_0^{\delta} \frac{\rho(x)}{1 + \omega\varepsilon_0\varepsilon\rho(x)} d(x) \quad (1)$$

The Power-Law impedance model for a CPE with a normal distribution is given in Eq. (1) and takes into account: resistivity dispersion ($\rho(x)$) among the paint thickness (δ) thanks to the integral function[23], the dielectric properties of the paint with a paint permittivity (ε) and the vacuum permittivity (ε_0) equal to 8.854×10^{-14} F.cm^{-2}. In this work, the paint is mainly made of epoxy resin, so we consider a constant permittivity (ε) of 3.6 for an epoxy-based paint[21]. The pulsation "ω" is considered equal to $2\pi f$ with f which representing the pulse frequency. This model considers the variation of the resistivity of the paint contrary to the simpler model still widely used and yet controversial of Hsu-Mansfeld[24], which considered the resistance of the paint as independent of the resistance of the electrolyte. This assumption is not valid in our case presumably because the resistance is linked to the porosity of the paint, and this resistance depends on the electrolyte unlike the capacitance, which depends on the dielectric characteristics of the paint itself[21]. Therefore, we use this Power-Law model to model the CPE_{paint}. In Fig. 2, we can observe a good agreement between the experimental points and the modelling of the impedance diagrams (Nyquist and Bode Fig. 2A, B respectively) with the EEC Power-Law model obtained with SIMAD® software validating the chosen EEC to represent a freshly paint hull.

Thanks to this model, a value of the porosity resistance ($R_{porosity}$) is estimated at around $2.2 \times 10^{+12} \pm 5.6 \times 10^{+11}$ Ω.cm^2. The very high value of this $R_{porosity}$ confirms once again the very protective and insulating character of this freshly deposited paint. The capacitance (C_{paint}) is estimated (Eq. 2) from the thickness of the paint (δ) considering the vacuum permittivity (ε_0) and the paint permittivity (ε) used for the Power-Law model (Eq. 1)[21].

$$C_{paint} = \frac{\varepsilon_0\varepsilon_{paint}}{\delta} \quad (2)$$

As the thickness of the paint is around 400 ± 150 µF, the capacitance is estimated equal to $8.1 \times 10^{-6} \pm 2.6 \times 10^{-6}$ µF.cm^{-2}. This value is consistent with the value of 6×10^{-6} µF.cm^{-2} reported in the book of Orazem Mark and Tribollet for an epoxy cast resin[21], confirming again the freshly painted carbon steel model presented in Fig. 3. Following these characterizations of a freshly painted sample, ageing measurements in synthetic seawater during 597 days are also analyzed.

Natural ageing of paint

The surface area investigated for this ageing test is larger than the one of the samples used for freshly painted electrochemical characterization (4.52 cm^2 vs to 2.2 cm^2 for freshly painted carbon steel) presented in the section "Experimental conditions" and used as reference for this study. Despite a larger area, a low current densities in the order of pA.cm^{-2} are measured, close to the detection limit of potentiostat. In order to accelerate ageing of the paint, anodic and cathodic overpolarizations at ±2 V vs E_{corr} are imposed, a well-known ageing technique in the literature[25,26]. These overpolarizations are carried out during three days at the beginning of the test (T0 + 2 days, 3 days, and 6 days) and increase slightly the current densities (up to 10 pA.cm^{-2}).

EIS results show as already reported in the results of other studies[19,22], a decrease of the low-frequency modulus (Fig. 4A) accompanied by a shift of the phase towards higher frequencies (Fig. 4B) with time. This behavior is characteristic of a loss of the barrier properties of the paint related to a progressive adsorption of water[19,26].

The interaction of seawater with the paint could lead to long-term degradation of the coating with the detachment of the paint from the metal substrate. This degradation is observed after the 597-days measurement as shown on the cross-section images obtained by backscattered electron imaging of the sample showing a lack of adherence of the paint (Fig. 5B). This detachment is not noticed for a freshly painted sample (Fig. 5A). No blister or other visual defects are observed at the surface of sample after running the experiment.

To model the aged painted metal/electrolyte interface and its time evolution, the same model as the one used for a freshly painted paint is proposed with the use of the Power Law as well. It appears that this model is valid for up to 48 days. The estimation of the EEC components (Fig. 3) confirm the degradation of the coating with a progressive reduction of $R_{porosity}$ and the increase of the parameter of the CPE (Q), which illustrate the loss of the barrier properties of the paint along time as shown in Table 1. The impedance of CPE (Z_{CPE}) depends on its two characteristic parameters, (α) and (Q) (Eq. 3)[21]:

$$Z_{CPE} = \frac{1}{Q(j\omega)^{\alpha}} \quad (3)$$

After 48 days, this model cannot be used anymore, as a second time constant appears. This second time constant is modelling by a resisto-capacitive element consisting of a non-ideal capacitance (CPE) and a resistor in parallel. A "α" parameter of about 0.5 is measured suggesting a porous electrode behavior as detailed by several authors[21,27]. This shows unambiguously infiltration of water through the paint to the metallic interface.

As a reminder, this first study focuses on the representation of painted steel surfaces in computational tool like CorOns. Generally, in the literature[3,6,28–30], only two states are considered

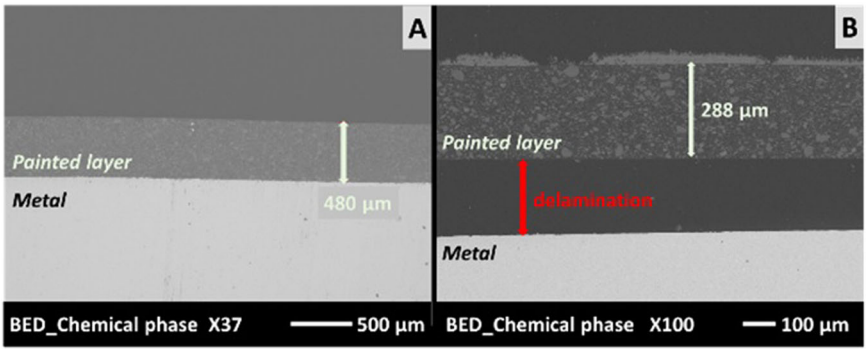

Fig. 5 Scanning Electron Microscope (SEM) pictures of different samples cross-sections at different stages of paint degradation. In (**A**), the case of freshly painted DH36 steel without defects and, in (**B**), a painted DH36 steel aged after 597 days of immersion. Both are immersed in artificial seawater at 20 °C naturally aerated in static condition. These images are obtained by Energy Dispersive X-ray Spectroscopy (EDS) using a Backscattered Electron Detector (BED).

Table 1. Estimated impedance parameters for the different components of the EEC representing the painted DH36 steel/artificial seawater interface during the first 48 days of immersion at 20 °C, in naturally aerated solution and static conditions with the estimated frequency range concerned by the CPE_{paint} phenomenon.

Time/days	CPE_{paint}		$R_{porosity}/\Omega.cm^2$
	α_{paint}	$Q_{paint}/F.cm^{-2}.s^{(\alpha-1)}$	
T0	0.97	3.0×10^{-11}	$3.6 \times 10^{+11}$
T0+2	0.96	3.5×10^{-11}	$8.5 \times 10^{+10}$
T0+3	0.95	3.9×10^{-11}	$6.5 \times 10^{+10}$
T0+6	0.96	4.2×10^{-11}	$3.3 \times 10^{+10}$
T0+27	0.95	4.6×10^{-11}	$1.4 \times 10^{+10}$
T0+48	0.96	4.4×10^{-11}	$2.9 \times 10^{+9}$

in cathodic protection modelling with computational tools: a freshly paint where the hull is represented by a pure insulator or a degraded paint taking into account a percentage of defects represented by unpainted surface. This work highlights the fact that these commonly used assumptions is too simple. Indeed, we highlight that a painted sample after some immersion time, even without visual defects, cannot be assimilated neither to a perfect insulator. V.G. DeGiorgi also mentions this aspect and the fact that defects cannot be simply represented by unpainted surfaces[30]. An intermediate model should be included to consider this state of degradation in computational tools like CorOns, to get closer to real-life conditions. After these first observations, the purpose is to study the impact of cathodic protection interruptions on the possible defect areas (unpainted surfaces) of ship hulls.

Defected surface (uncovered surface) under cathodic protection

Following these observations, we are interested in the corrosion processes happening at the level of the defects (unpainted zone) under cathodic protection in order to improve the current computational simulation. In that case, an unpainted sample is cathodically polarized with an applied potential at −0.8 V vs SCE. This potential is 50 mV lower with respect to the corrosion potential ("E_{corr}") equal to −0.72 V vs SCE for the studied DH36 steel. After 7 days of maintainance at this potential, the beginning of calcareous deposit formation is observed as reported in several studies[12–14].

After these 7 days, we can observe the beginning of Ca-rich agglomerate formation[14,17]. According to Fig. 6E, C, these agglomerates are mainly composed of calcium and oxygen as already reported by numerous works based on this deposit[12–14]. Indeed, authors observe a Ca carbonate layer formation as outer layer after several days under cathodic protection. Its formation kinetic depends on the electrolyte composition and applied potentials[12–14].

This outer layer should have better barrier properties in comparison with the Mg-hydroxides-rich inner layer, according to the review of Carré et al.[13]. As a result, a decrease in current densities should be observed[12–14]. Here, we do not observe a clear decrease in current densities Fig. 7 suggesting a partial covering of the surface.

We do observe the first layer rich in magnesium hydroxides/corrosion products that is present at the interface between the agglomerate and the metal surface, as seen in Fig. 6B, D. The Mg mapping, despite being very noisy, is seem to show high concentration of magnesium at the base of the agglomerates: very thin layer <2 µm (Fig. 6B). All these observations are consistent with the literature, which investigate the formation of a calcareous deposit and its corrosion barrier properties[12–14,17].

This observation is confirmed by the EIS measurements which showed an increase in modulus at low frequency with the growth a progressive recovery of the calcareous deposit on the surface (Fig. 8A). In parallel, the phase decreases (loss of the capacitive behavior) and after 4 days under cathodic polarization two peaks can be distinguished at high frequency between 1 kHz and 10 kHz and at intermediate frequency, 1–10 Hz (Fig. 8B). This suggests, at least two times constants, which can be related to the faradic phenomena at the seawater/metal interface and to the dielectric properties of the calcareous deposit. In some works[11,12], two layers of the calcareous deposit are distinguished by impedance spectroscopy, but in our case, the calcium carbonate layer (outer layer) might not cover the whole surface of the sample.

This may explain the single high-frequency contribution (1 kHz to 10 kHz) attributed to the deposit. The EEC proposed, is a double "R // CPE" system in parallel as represented in Fig. 9, as suggested by the semicircle shape of EIS diagram on Nyquist representation Fig. 10[21]. A diffusion impedance (Warbrug model[31]) is added in series with the transfer resistance because, at this applied potential (−0.8 V vs SCE) according to the polarization curve (Fig. 7) the system is limiting by oxygen diffusion[13,14,17].

Impedance spectra (Fig. 9) show quite great superposition between EEC fit and the experimental data, as presented with the Nyquist diagram Fig. 10. In the model Fig. 9, we consider a dispersion of time constants based on the heterogeneities in terms of thickness, composition, and covering of the deposit and this covering on the metal surface, consequently a CPE is used rather than pure capacitance. For the fitting of the intermediate phenomenon attributed to faradic phenomenon, an estimation of the capacitance value and resistance and its evolution during the

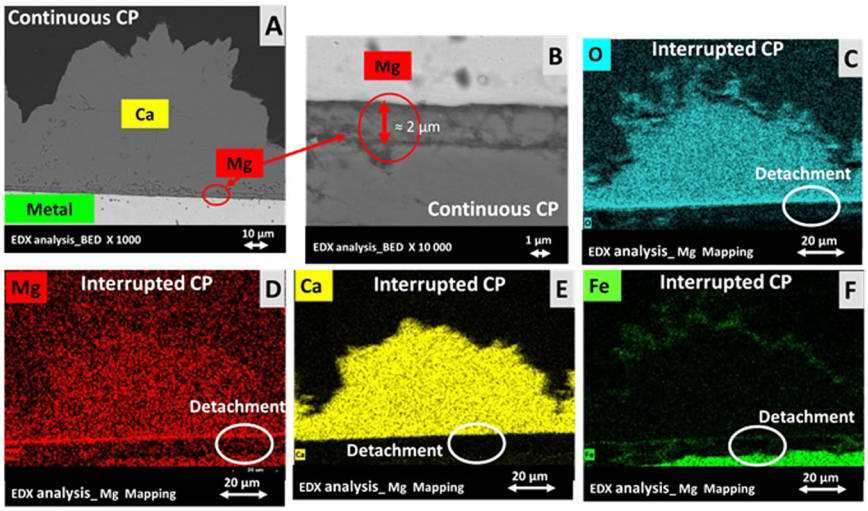

Fig. 6 SEM pictures of the seawater/metal interface state during continuous or interrupted cathodic protection. In (**A**, **B**), cross-sections of the sample obtain after continuous cathodic protection for 7 days in natural aeration, at 20 °C in static conditions. In (**C**–**F**), cross-sections pictures of a sample obtain after two interruptions of the cathodic protection, in natural aeration, at 20 °C, under static conditions. EDX mapping of the elements is performed.

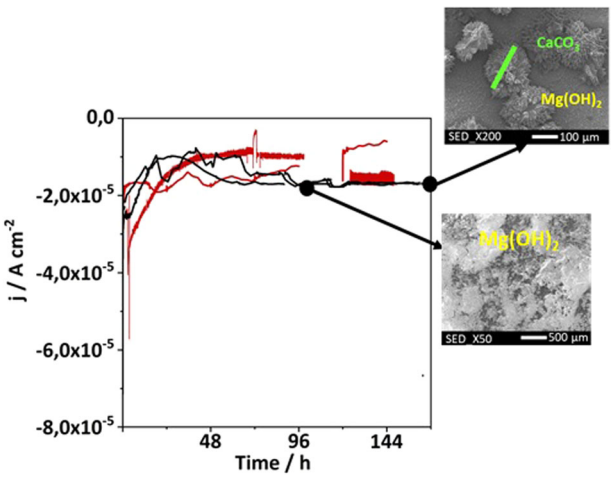

Fig. 7 Monitoring of the current density during 7 days of continuous or interrupted cathodic polarization of DH36 steel immersed in seawater. The "black curve" represents the current density in function of the time for continuous cathodic polarization with the topography of the sample surface after 4 days and 7 days (SEM pictures), and the "red curve" represents the current density in function of the time for interrupted cathodic polarization. Both cases are realized at 20 °C, natural aeration conditions and static conditions.

7 days is done thanks to the use of EC-LAB® software. These phenomena are represented by a double-layer capacitance and a charge transfer resistance related to the oxygen reduction reaction.

To estimate the double-layer capacitance value, the Brug's equation law is used for the faradic phenomena[21]. Indeed, we consider a surface distribution of the time constants because of the geometric irregularities of the interface observed due to the presence of calcareous deposit. Characteristic range value for a double-layer capacitance according to Loveday et al.[32] and Tribollet and Orazem book[21], is between 50 and 100 µF.cm^{-2}[19]. Figure 11 shows the progressive decrease of the double-layer capacitance and the increase of the charge transfer resistance suggesting the progressive growth of the calcareous deposit and the progressive covering of the surface. However, the capacitance remains quite high, between 70 and 50 µF.cm^{-2} during the first 4 days. A capacitance value of this range suggests an active surface, i.e., the formed deposit is not enough for covering and dense to limit the corrosion process[21]. Hence, the EEC model could be simplified for the first few days of immersion neglecting $C_{deposit}$ and $R_{porosity}$ (Fig. 11A).

Following these first observations, we also study the impact of the stop of the cathodic protection on this calcareous deposit. For this purpose, 24 h stops of the cathodic protection are carried out on the 5th day (96–120 h period) and the 7th day (144–168 h period) with a restart on the 6th day (120–144 h period). At the end of the first 24 h of stop, the impedance response is represented by the red curves in Fig. 12. During the 6th day, the cathodic protection is restarted and after 24 h (T0 + 144 h), the green curve is obtained (Fig. 12).

Consequently, to the stop of the cathodic protection system, a degradation of the metal/deposit interface is noticed with a detachment of the calcareous deposit (Fig. 6B). This loss of adhesion is not observed in the case of samples continuously polarized during 7 days.

However, the structure of the calcareous deposit is similar with an inner layer made of $Mg(OH)_2$ and an outer layer made of $CaCO_3$ agglomerated, according to the EDX/MEB mapping performed on both types of samples. The calcareous deposit formation steps do not seem disturbed by these interruptions allowing using the same EEC model (Fig. 9) to represent our interface.

Loss of protective properties of this deposit is observed by impedance spectroscopy. The Bode diagram shows a gradual increase of the 10 mHz modulus during the first 4 days (Fig. 12A) suggesting the formation and the progressive covering of the surface by the calcareous deposit. The phase variation (Fig. 12B), indicates at least two times constants with: after 4 days under cathodic protection, a phenomenon relaxing between 0.1 Hz and 10 Hz, which could be attributed to the faradic phenomena and at high frequencies, around 10 kHz, another phenomenon that would correspond rather to the more and more covering deposit. These observations are in agreement with those made on a 7-day polarization presented previously.

However, in this case, both contributions are clearly distinguished after the first 24 h cut-off. Indeed, a first peak, associated to the dielectric properties of the calcareous deposit between 100 Hz and 1 kHz, which do not change, whereas the second phenomenon (between 0.1 Hz and 10 Hz) would be associated

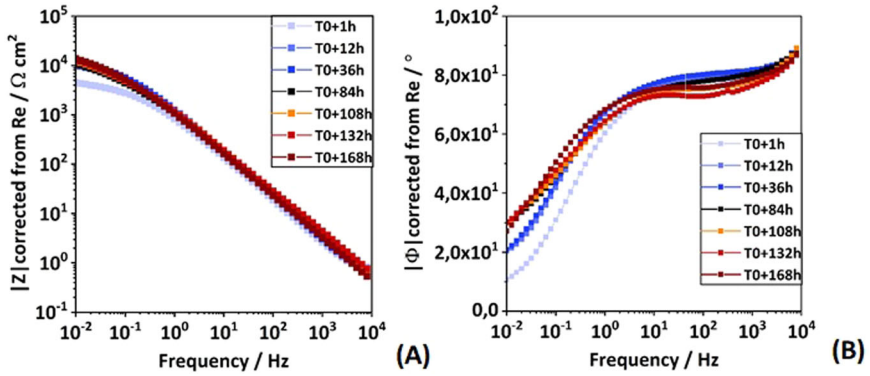

Fig. 8 Bode diagrams measured regularly during 7 days of continuous cathodic polarization at −0.8 V vs SCE of DH36 steel. The modulus in (**A**) and phase in (**B**) are plotted in function of the frequency and corrected for Re (electrolyte resistance). Measurements are made after 1 h, 12 h, 36 h, 84 h, 108 h, 132 h, and 168 h of immersion at 20 °C, under static condition and natural aeration.

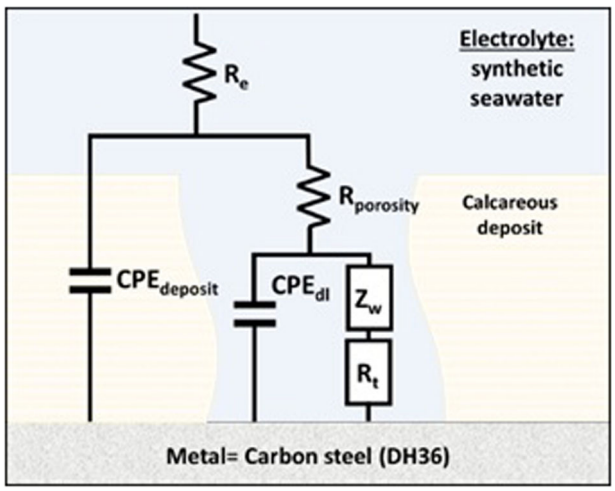

Fig. 9 The EEC model represents the interface of unpainted DH36 steel/seawater under continuous or interrupted cathodic protection. This EEC model is valid at room temperature, under static conditions, and with artificial naturally aerated seawater.

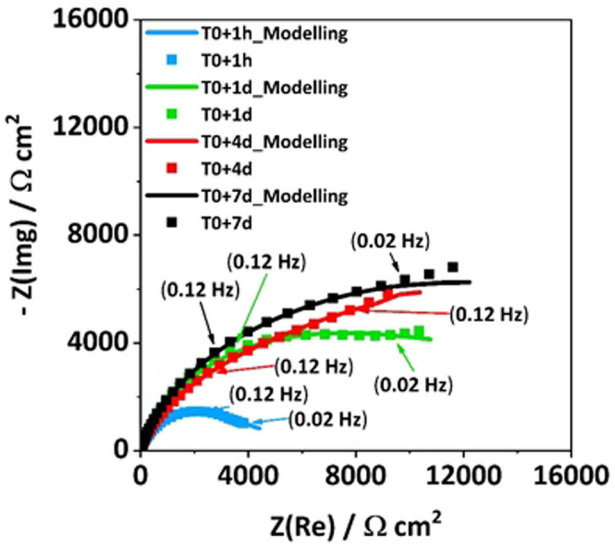

Fig. 10 Nyquist diagrams measured during 7 days of cathodic polarization at −0.8 V versus SCE. Imaginary (Z(img)) is plotted in function of the real parts (Z(Re)) of the impedance, under static, at 20 °C in natural aeration and static conditions, after 1 h, 1 day, 4 days and 7 days of continuous cathodic polarization.

with the faradic process, seem to shift towards lower frequencies. This indicates an acceleration of the corrosion process which could be related to the embrittlement of the calcareous deposit and a loss of its corrosion barrier properties.

The presence of two times constants, as in the continuous polarization case, reinforces the hypothesis of using the same EEC model (Fig. 9) and is further confirmed by great correlation between experimental and modeled data. Considering this model (Fig. 9), we have investigated the impact of the cut-off on the faradic contribution and the evolution of the double-layer capacitance, the faradic impedance, and the diffusion phenomenon.

Figure 13 reports the evolution of the capacitance, the charge transfer resistance and "σ_w", the Warburg impedance characteristic parameter describes by Diard et al.[31].

During polarization stops, "Rt" is replaced by a global faradic impedance "Z_f" at open circuit when the system is not limited by only on phenomenon[21], as general corrosion takes place at E_{corr}. In this case, it will be more relevant to use a global impedance representing all the processes.

This modelling of impedance diagrams highlights the loss of calcareous deposit protective behavior with the faradic impedance or "Rt" under cathodic protection, as the phase strongly decreases (almost a decade) after the first 24 h of "ICCP off" (Fig. 14C). Then, it does not increase afterwards, indicating a permanent loss of the barrier properties of this deposit related to an increase of active area due to electrolyte infiltration under the deposit. Consequently, corrosion become localized with the formation of electrochemical cell created between the different aerated areas: for example, between active area under the deposit and the one in uncovered area. This notion of active area associated to moisten zones responsible of localized corrosion is presented in several works, which talk about induce passivation and residual protection after cut-off of the CP system in soil[33–36]. In our case, we don't observe an induced passivation phenomenon during the cut-off period of cathodic protection. Instead, we observe a direct progressive discharge phenomenon seem to be present, related to a residual protection due to the calcareous deposit which is a novelty for this targeted application. According to potential monitoring, we can observe as mentioned in the work of Wang et al.[35], that the "potential shift toward less noble direction", related to the capacitive charging/discharging could be associated with the presence of the calcareous deposit (T0 + 96–120 h period).

As observed in Fig. 15, the potential decreases progressively toward the corrosion potential of an unprotected plate estimated around −0.72 ± 0.01 V vs SCE. This discharge

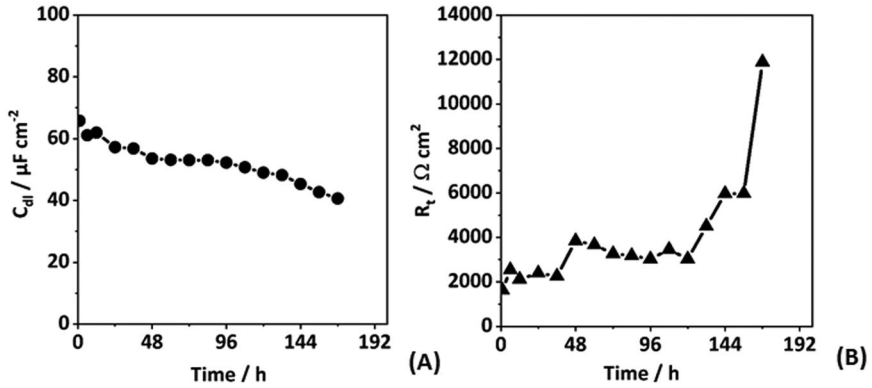

Fig. 11 EEC model parameters evolution during the 7 days of continuous cathodic polarization. Double-layer capacitance (Cdl) estimated with the Brug law's in (**A**) and a charge transfer resistance (Rt) in (**B**) in function of time and estimated from EIS data measured with EC-LAB® software modelling, in static conditions, natural aeration, and 20 °C.

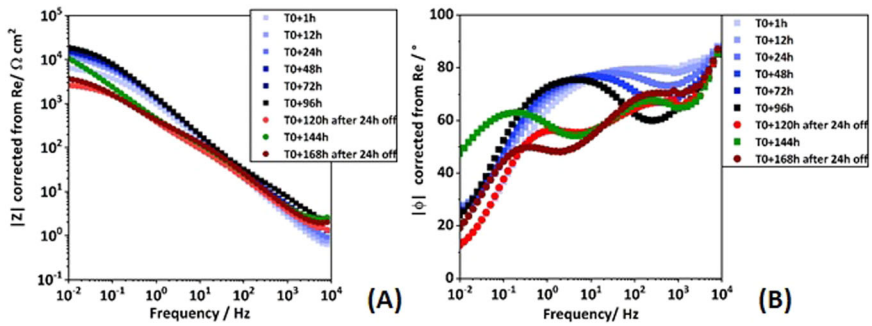

Fig. 12 Bode diagrams obtained regularly during the 7 days of cathodic polarization with two interrupted phases (the 5th and 7th days). The modulus in (**A**) and phase in (**B**) are plotted in function of the frequency and corrected from the "Re" (Electrolyte Résistance), for unpainted DH36 steel immersed in naturally aerated artificial seawater and in static conditions at 20 °C.

phenomenon seems to be shorter after the second CP interruption (T0 + 144 h–168 h period) which can be linked to loss of covering and protecting properties of the calcareous deposit.

The parameter "σ_w" in Fig. 14C, corresponding to the Warburg-type diffusion impedance practically disappears (*closed to 0*) during the interruption phases. This would be consistent with the fact that at open circuit potential, the system would be almost no longer limited by O_2 diffusion in correlation with the loss of the protection efficiency.

The double-layer capacitance values measures, after the 24-h cathodic protection interruptions, were very high around 100 µF.cm^{-2} (Fig. 14A). This very high value suggests the presence of additional phenomena, undistinguishable in our conditions of the study. This could be due to the infiltration of seawater under the calcareous deposit as presented in the work of Ben Amor et al.[37]. This idea is reinforced by estimated values of C_{dl} around 70 µF.cm^{-2}, which is still very high and characteristic of a total active area when the cathodic protection is reactivated during the 6th day (Fig. 14A). This confirms once again the calcareous barrier properties loss.

From this study, several points are observed that could improve the CorOns computational tool for ship electrical signature simulations:

- Short interruption of cathodic protection system does not affect current density demand.
- In the long term, an accelerated degradation of the deposits formed on the surface of the materials could be expected following several interruptions of the cathodic protection system with a possible evolution of the currents and thus the electrical signatures.

METHODS

Experimental conditions

To represent the ship's hull material, DH36 carbon steel discs are used. The detailed composition of DH36 alloy is presented in Table 2. Coated sample size is 3 cm in diameter and for uncoated sample 1 cm in diameter, with 5 mm in thickness for both sample's type.

Samples are polished with SiC paper up 1200 grit. The samples are degreased in an ethanol and acetone bath under ultrasound for 5 min, to ensure good reproducibly of the surface between each experiment.

The case of an undamaged hull is representing, at the laboratory scale, by a sample of DH36 steel coated with a fresh layer of Hempel's first undercoat®. This undercoat®paint corresponds to the first anticorrosion layer applied in real conditions, on vessels. This layer has demonstrated high protection by itself at this scale. The paint is applied with an airbrush and the thickness is estimated to be around 400 ± 150 µm. Thicknesses are measured by image analysis from optical microscope images on four different places of the samples and a mean value with a standard deviation (error) are estimated. An estimated immersing area of 2.2 cm^2 is measured for painted samples.

High level of the damaged area is represented by unpainted sample. The electrochemical behavior of our materials is investigated in synthetic seawater prepared according to ASTM1141-98 (2013)[38]. The seawater composition is given in Table 3 below:

Electrochemical measurements are recorded using a classical 3-electrodes system with a platinum mesh as counter electrode, a Saturated Calomel Electrode reference (SCE) and the sample as the working electrode. The exposed surface is controlled thanks to a gasket on the sample holder.

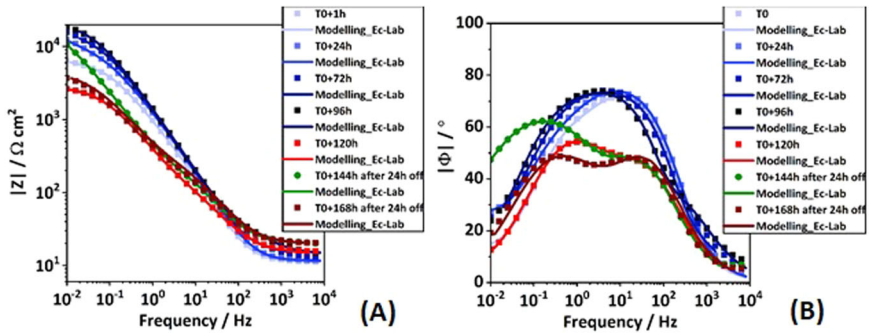

Fig. 13 Superposition of the experimental Bode diagrams and the Bode diagrams modelling with the EC-LAB® software, obtained regularly during the 7 days of cathodic polarization with two interrupted phases (during the 5th and 7th days). The modulus in (**A**) and the phase in (**B**) are plotted in function of the frequency during 7 days of cathodic polarization with 2 days of interruptions (5th and 7th days) for an unpainted DH36 steel immersed in naturally aerated artificial seawater, under static conditions at 20 °C.

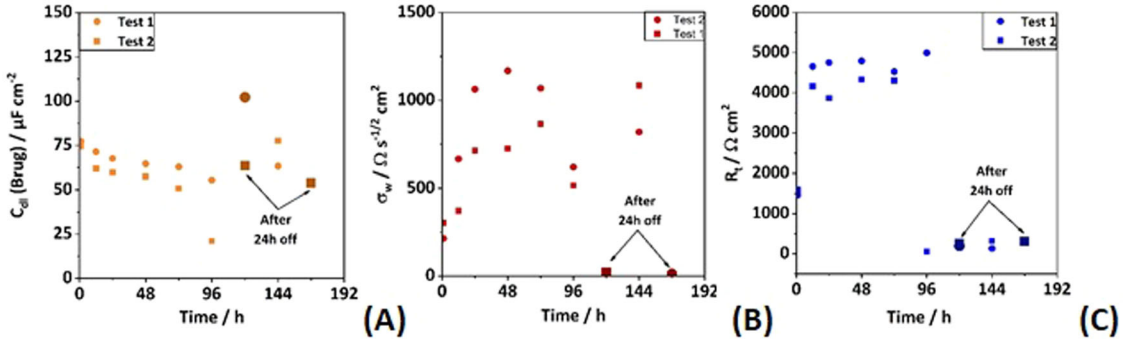

Fig. 14 Progression of the EEC parameters during the 7 days of cathodic polarization with two days of interruption (the 5th and 7th days). The double layer capacitance (Cdl) estimated with Brug's law in (**A**), the Warbrug constant for the diffusion phenomenon (σ_w) in (**B**), and the charge transfer resistance ($R_{t)}$ or the faradic impedance (Z_f) in (**C**), for an unpainted DH36 steel immersed for 7 days in a naturally aerated solution, in a static condition at 20 °C.

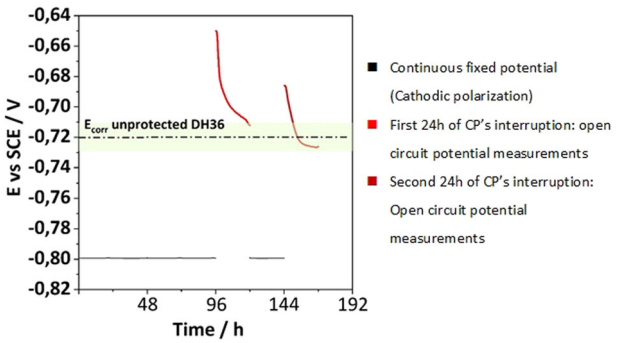

Fig. 15 Monitoring of the potential at the DH36 surface under on/off period of cathodic protection. Potential ate DH36 surface in the function of the time, at 20 °C, static conditions and in natural aeration condition.

A fourth electrode (platinum wire + 1 µF capacitor arranged in series) is placed in parallel with the reference electrode to filter high-frequency signals (high-pass filter[39]). A Faraday box is also used to avoid external electrical perturbations. To perform experimental measurements, a Gamry Ref 600 potentiostat is used. The measurements are recorded under static conditions, natural aeration (*open electrochemical cell*), and at controlled room temperature (20 °C).

Ageing test of 597 days in artificial seawater

Ageing measurements are performed at 20 °C in artificial seawater with a sample surface area of 4.52 cm^2. The sequence of measurements consists in recording the open circuit potential also referred as the corrosion potential, often designated by "E_{corr}", during 2 h. Once stabilized, an electrochemical impedance spectroscopy (EIS) measurement is recorded at E_{corr}. The amplitude of the Alternative Current, "AC" signal is ±10 mV with a frequency range between 10 mHz and 10 kHz. The chosen frequency range often used in the literature, is 10 mHz–100 kHz[11,40,41] for these kinds of experiments. However, in our case, despite faraday cage and reference derivation (1 µF capacitance), our impedance signals are perturbed and illegible after 10 kHz. Faraday cage and fourth electrode (High-pass filter on reference, cf. page 4 section 2.1) allow us to eliminate 50 µHz perturbation's related to external electrical installation and to obtain better high-frequency signals with a higher limit: 10 KHz instead of 1 kHz.

Finally, a potentiodynamic measurement is carried out from ±30 mV vs E_{corr} to ±500 mV vs E_{corr} with a sweeping rate of 0.2 mV. s^{-1}. This sequence of measurements is running every 2 weeks during the 597 days of experiments to follow the ageing of paints[19,32]. A single test is performed for this experiment. The result obtained is compared with the results obtained with freshly used samples as reference. Freshly painted samples are characterized with only 2 h OCP and then an impedance measurement with the same parameters as those used for the aging test. This reference test is performed at least 3 times.

Cathodic protection protocol

To simulate the effect of cathodic protection on defects or unpainted areas of a hull, samples without paint are cathodically polarized during 7 days as previously reported[11,13,14,42]. To do so a

Table 2. Chemical composition of DH36 steel used as the hull material.

DH36	C	Mn	Si	P	S	Cu	Ni	Cr	Mo	Al	V	Nd	Ti	Fr
%Wt	0.18	0.9–1.6	0.5	0.03–5	0.03–5	0.35	0.4	0.2	0.08	0.02	0.05–0.1	0.02–0.05	0.02	Bal.

Table 3. Chemical composition of synthetic seawater following ASTM-98 (2013) standard[38].

Ions	Cl^-	Na^+	SO_4^{2-}	Mg^{2+}	Ca^{2+}	K^+	HCO_3^-	Br^-
Concentration/g.L^{-1}	19.08	11.03	2.77	1.33	0.42	0.40	0.15	0.07

fixed potential of −0.8 V vs SCE is applied to the samples according to AFNOR NF EN 16222 standard[42]. Regular EIS measurements are recorded (at T0 + 2 h, 6 h, 12 h, and every 12 h after) at this protection potential with an Alternative Current of ±10 mV and a frequency range between 10 mHz and 10 kHz (same parameters as ageing test) on a 0.45 cm^2 sample. According to several works[11,14,17,40–42], this protocol and frequency range, is considered appropriate to follow the interface changes and deposit growth.

Surface characterization and EIS investigation

For the whole study presented here, two computational software are used for impedance modelling: SIMAD® and EC-LAB®. SIMAD® software is a homemade software developed at the "Laboratoire Interfaces et Systèmes Electrochimiques" at "Pierre et Marie Curie University (UMPC)" in France. EC-LAB® software is developed by the Biologic® Company. Both software are developed to model impedance datas (diagram), thank to Electrical Equivalent Circuit and analytical expressions.

The SIMAD® software is used as power-law model could be implemented to fit EIS data in comparison with EC-LAB® software that is a commercial one in which we could not use power-law model. Three repetitions are realized for each test (continuous or intermittent cathodic protection).

To characterize the metallic interfaces, SEM (*Scanning Electron Microscopes*) measurements are performed with FEG-SEM JEOL® (*Field Emission Gun-Scanning Electron Microscopes*) equipped with an energy-dispersive X-ray detector (*Energy Dispersive X-ray spectroscopy detector – Bruker Nano XFlash 6|60*). EDX measurements are also performed to determine qualitatively the different chemical elements present at the metal/electrolyte interface.

DATA AVAILABILITY

The datasets generated during and/or analyzed during the current study are available from the corresponding author on reasonable request.

CODE AVAILABILITY

This purely experimental work did not use any specific software code different from the one used by EC-LAB® and SIMAD® software.

Received: 20 October 2022; Accepted: 9 March 2023;
Published online: 06 April 2023

REFERENCES

1. Daya, Z. A., Hutt, D. L. & Richards, T. C. *Maritime Electromagnetism and DRDC Signature Management Research* 80 (2005).
2. Demilier, L. et al. in *Simulation of Electrochemical Processes II* Vol. I, 235–244 (WIT Press, 2007).
3. DeGiorgi, V. G., Hogan, E., Lucas, K. E. & Wimmer, S. A. in *WIT Transactions on State of the Art in Science and Engineering* (ed. Adey, R. A.) Vol. 1, 13–44 (WIT Press, 2005).
4. Guibert, A., Chadebec, O., Coulomb, J.-L., Rannou, C. & Nogueira, R. P. Ships hull corrosion diagnosis from close measurements of electric potential in the water. *Eur. Phys. J. Appl. Phys.* **52**, 23310 (2010).
5. Kim, Y.-S., Lee, S. K. & Kim, J.-G. Influence of anode location and quantity for the reduction of underwater electric fields under cathodic protection. *Ocean Eng.* **163**, 476–482 (2018).
6. Xing, S. H., Li, Y., Song, H. Q., Yan, Y. G. & Sun, M. X. Optimization the quantity, locations and output currents of anodes to improve cathodic protection effect of semi-submersible crane vessel. *Ocean Eng.* **113**, 144–150 (2016).
7. Nale, M. et al. Transient Modelling of Corrosion Protection Systems with BEM-Electrical Circuit Hybrid Model. *IEEE Trans. Magn.* (2023)
8. Nale, M. Développement et validation de modèles transitoires et multi-échelles de signatures électriques sous-marines de navires. Energie électrique. Université Grenoble Alpes, (2022).
9. DeGiorgi, V. G., Thomas, E. D. III & Lucas, K. E. Scale effects and verification of modeling of ship cathodic protection systems. *Eng. Anal. Bound. Elem.* **22**, 41–49 (1998).
10. Kim, Y.-S., Lee, S. K., Chung, H.-J. & Kim, J.-G. Influence of a simulated deep sea condition on the cathodic protection and electric field of an underwater vehicle. *Ocean Eng.* **148**, 223–233 (2018).
11. Hong, M.-S., Hwang, J.-H. & Kim, J. H. Optimization of the cathodic protection design in consideration of the temperature variation for offshore structures. *Corrosion* **74**, 123–133 (2018).
12. Karoui, H. et al. Electrochemical scaling of stainless steel in artificial seawater: role of experimental conditions on CaCO3 and Mg(OH)2 formation. *Desalination* **311**, 234–240 (2013).
13. Carré, C. et al. Electrochemical calcareous deposition in seawater. A review. *Environ. Chem. Lett.* **18**, 1193–1208 (2020).
14. Barchiche, C. et al. Characterization of calcareous deposits in artificial seawater by impedance techniques. *Electrochimica Acta* **48**, 1645–1654 (2003).
15. Yan, J. -F., White, R. E. & Griffin, R. B. Parametric studies of the formation of calcareous deposits on cathodically protected steel in seawater. *J. Electrochem. Soc.* **140**, 1275–1280 (1993).
16. Yang, Y., Scantlebury, J. & Koroleva, E. A study of calcareous deposits on cathodically protected mild steel in artificial seawater. *Metals* **5**, 439–456 (2015).
17. Barchiche, C., Deslouis, C., Gil, O., Refait, P. & Tribollet, B. Characterisation of calcareous deposits by electrochemical methods: role of sulphates, calcium concentration and temperature. *Electrochimica Acta* **49**, 2833–2839 (2004).
18. Zamanzade, M., Shahrabi, T. & Yazdian, A. Improvement of corrosion protection properties of calcareous deposits on carbon steel by pulse cathodic protection in artificial sea water. *Anti-Corros. Methods Mater* **54**, 74–81 (2007).
19. Loveday, D., Peterson, P. & Rodgers, B. Evaluation of organic coatings with electrochemical impedance spectroscopy: Part 2: Application of EIS to coatings. *JCT CoatingsTech* **6**, 88–93 (2005).
20. Mahdavian, M. & Attar, M. M. Another approach in analysis of paint coatings with EIS measurement: phase angle at high frequencies. *Corros. Sci.* **48**, 4152–4157 (2006).
21. Orazem Mark, E. & Tribollet, B. *Electrochemical Impedance Spectroscopy* (Wiley, 2008).
22. Touzain, S., Thu, Q. L. & Bonnet, G. Evaluation of thick organic coatings degradation in seawater using cathodic protection and thermally accelerated tests. *Prog. Org. Coat.* **52**, 311–319 (2005).
23. Hirschorn, B. et al. Constant-Phase-Element behavior caused by resistivity distributions in film. *J. Electrochem. Soc.* **157**, C458 (2010).
24. Orazem, M. E. et al. Dielectric properties of materials showing constant-phase-element (CPE) impedance response. *J. Electrochem. Soc.* **160**, C215–C225 (2013).
25. Loveday, D., Peterson, P. & Rodgers, B. Evaluation of organic coatings with electrochemical impedance spectroscopy: Part 3: Protocol for testing coating with EIS. *JCT CoatingsTech* **2**, 22–27 (2005).

26. Martinez, S., Žulj, L. V. & Kapor, F. Disbonding of underwater-cured epoxy coating caused by cathodic protection current. *Corros. Sci.* **51**, 2253–2258 (2009).
27. Amor, Y. B., Sutter, E. M. M., Takenouti, H., Orazem, M. E. & Tribollet, B. Interpretation of electrochemical impedance for corrosion of a coated silver film in terms of a pore-in-pore model. *J. Electrochem. Soc.* **161**, C573–C579 (2014).
28. Xing, S., Wu, J. & Yan, Y. Optimization of a ship's ICCP system to minimize electrical and magnetic signature by mathematical simulation. 69–77 (2009).
29. Wu, J., Xing, S., Liang, C., Lu, L. & Yan, Y. The influence of electrode position and output current on the corrosion related electro-magnetic field of ship. *Adv. Eng. Softw.* **42**, 902–909 (2011).
30. DeGiorgi, V. G. Evaluation of perfect paint assumptions in modeling of cathodic protection systems. *Eng. Anal. Bound. Elem.* **26**, 435–445 (2002).
31. Diard, J.-P., Le Gorrec, B. & Montella, C. *Cinétique électrochimique* (Hermann, 1996).
32. Loveday, D., Peterson, P. & Rodgers, B. Evaluation of organic coatings with electrochemical impedance spectroscopy: Part 1: Fondamentals of electrochemical impedance spectroscopy. *JCT CoatingsTech* **6**, 46–52 (2004).
33. Nguyen Dang, D., Lanarde, L., Jeannin, M., Sabot, R. & Refait, P. Influence of soil moisture on the residual corrosion rates of buried carbon steel structures under cathodic protection. *Electrochimica Acta* **176**, 1410–1419 (2015).
34. Akkouche, R. et al. Influence of soil moisture on the corrosion processes of carbon steel in artificial soil: active area and differential aeration cells. *Electrochim. Acta* **213**, 698–708 (2016).
35. Wang, K., Varela, F. B. & Tan, M. Y. The effect of electrode surface area on corrosion initiation monitoring of X65 steel in soil. *Corros. Sci.* **152**, 218–225 (2019).
36. Akkouche, R. et al. Electrochemical monitoring of steel/soil interfaces during wet/dry cycles. *J. Electrochem. Soc.* **164**, C626–C634 (2017).
37. Ben Amor, Y., Bousselmi, L., Tribollet, B. & Triki, E. Study of the effect of magnesium concentration on the deposit of allotropic forms of calcium carbonate and related carbon steel interface behavior. *Electrochim. Acta* **55**, 4820–4826 (2010).
38. American Society for Testing and Materials. Standard practice for the preparation of substitute ocean water. ASTM International (2013).
39. Sadkowski, A. & Diard, J.-P. On the Fletcher's two-terminal equivalent network of a three-terminal electrochemical cell. *Electrochem. Acta* **55**, 1907–19011 (2010).
40. Hoseinieh, S. M., Shahrabi, T., Ramezanzadeh, B. & Rad, M. F. The role of porosity and surface morphology of calcium carbonate deposits on the corrosion behavior of unprotected API 5 L X52 rotating disk electrodes in artificial seawater. *J. Electrochem. Soc* **163**, C515–C529 (2016).
41. Izadi, M., Yazdiyan, A., Shahrabi, T., Hoseinieh, S. M. & Shahrabi, H. Influence of temperature variation on the formation and corrosion protective performance of calcium carbonate deposits in artificial seawater. *J. Mater. Eng. Perform.* **28**, 4221–4233 (2019).
42. Protection cathodique des coques de bateaux_NF EN 16222, *national standard AFNOR* (2012).

ACKNOWLEDGEMENTS

The authors acknowledge all the actors who have contributed to this research like the French Navy for the financial support and the CNRS.

AUTHOR CONTRIBUTIONS

M.M.: Conceptualization, methodology, investigation, formal analysis, writing—review & editing. V.R.: Conceptualization, methodology, resources, formal analysis, writing—review & editing, supervision. J.C.L.: Methodology, investigation, writing—review & editing. O.P., L.-L.R., O.C., and M.N.: Editing, collaboration specialists in modelling of electromagnetic signatures of ships and the development of numerical tools for this purpose like the CorOns software C. Goëau, also specialized in the measurement of electromagnetic signatures of ships in real conditions. The French Navy "Direction Générale de l'Armement" in collaboration with the "Centre National de Recherche Scientifique", the University of Grenoble Alpes, and the "Institut Polytechnique de Grenoble" supported these works.

COMPETING INTERESTS

The authors declare no competing interests.

ADDITIONAL INFORMATION

Correspondence and requests for materials should be addressed to Marie Minola or Virginie Roche.

Reprints and permission information is available at http://www.nature.com/reprints

Publisher's note Springer Nature remains neutral with regard to jurisdictional claims in published maps and institutional affiliations.